Journal of Organometallic Chemistry 920 (2020) 121336

Contents lists available at ScienceDirect

Journal of Organometallic Chemistry

journal homepage: www.elsevier.com/locate/jorganchem

Synthesis of ferrocenylated-aminopyridines and ferrocenylated-aminothiazoles and their anti-migration and burning rate catalytic properties

Muhammad Usman [a], Haojie Yu [a, **], Li Wang [a, *], Pavel A. Zhizhko [b], Dmitry A. Lemenovskiy [c], Dmitry N. Zarubin [b], Amin Khan [a], Kaleem-ur-Rehman Naveed [a], Ahsan Nazir [a], Shah Fahad [a]

[a] State Key Laboratory of Chemical Engineering, College of Chemical and Biological Engineering, Zhejiang University, Hangzhou, 310027, PR China
[b] A.N. Nesmeyanov Institute of Organoelement Compounds, Russian Academy of Sciences, Vavilov Str., 28, 119991, Moscow, Russia
[c] Department of Chemistry, Moscow State University, Vorob'evy Gory 1, 119992, Moscow, Russia

ARTICLE INFO

Article history:
Received 14 November 2019
Received in revised form
16 April 2020
Accepted 4 May 2020
Available online xxx

Keywords:
Ferrocene
Burning rate catalysts
Anti-migration behavior

ABSTRACT

For overcoming the migration problems of ferrocene (Fc)-based burning rate catalysts (BRCs) as well as for enhancing burning rate (BR) of ammonium perchlorate (AP)-based propellants, ferrocenylated-amino pyridines (AP-Fcs) and ferrocenylated-amino thiazoles (AT-Fcs) have been synthesized. The synthesis of AP-Fcs and AT-Fcs was confirmed by nuclear magnetic resonance (^{1}H NMR). Electrochemical properties of these ferrocenylated derivatives were explored by cyclic voltammetry (CV). The BR catalytic activities of AP-Fcs and AT-Fcs on thermal decomposition of AP were examined by thermogravimetric (TG) and differential thermogravimetric (DTG) techniques. Thermal analysis results showed that AP-Fcs and AT-Fcs showed good BR catalytic effects on thermal decomposition of AP. AP-Fcs and AT-Fcs were also applied for anti-migration studies in comparison with catocene (Cat) and ferrocene. It was found that AP-Fcs and AT-Fcs displayed anti-migratory behavior.

1. Introduction

Propellants are considered as the key contributors in missile and space technology. They provide driving force for rockets and missiles [1–3]. Most of the solid propellants are combination of chemical ingredients such as pre-polymers, curatives, plasticizers, antioxidants, burning-rate (BR) modifiers, catalysts, and oxidizers [4]. AP is the extensively utilized oxidizer in solid propellants by virtue of its exceptional combustion characteristics, ease in processibility and storability. Since AP usually accounts for 60–90% of the composite solid propellants, therefore the thermal decomposition of AP directly influences the burning velocity [5–7]. The thermal disintegration of AP is considered to have a strong effect on the combustion process of the propellants [8–13]. So, it is vital to improve the thermal decomposition efficiency of AP. The thermal decomposition of AP can be accelerated by adding burning rate catalysts (BRCs) in solid propellants [14–16].

Ferrocene and its derivatives in recent times have received much attention due to their thermal stabilities, excellent redox behaviors and good catalytic properties [17–23]. Therefore they are widely used in various fields such as medicines [24], electrochemical sensors [25], memory storage devices [26–29], nanomaterials [30–36], and catalysis [37–42] etc. Since catalysis is an important feature of ferrocene-based derivatives therefore, they have been verified as the most effective catalysts for AP-based composite solid propellants [43].

Ferrocene-based BRCs are superior than other BRCs (for example metal oxides, metal coordination polymers, nano-composites and carbon materials) [14] due to their good compatibility with organic binder and uniform microscopic distribution in the propellant, better fluidity and better ignitability of the propellant [44]. Ferrocene-based BRCs are capable to enhance burning rates and bringing down the pressure indexes of the propellants during combustion [45]. The current commercially available ferrocene-based BRCs such as 2,2-bis(ethylferrocenyl)propane (catocene), *tert*-butylferrocene (TBF) and *n*-butylferrocene (NBF) are neutral

* Corresponding author.
** Corresponding author.
E-mail addresses: hjyu@zju.edu.cn (H. Yu), opl_wl@dial.zju.edu.cn (L. Wang).

https://doi.org/10.1016/j.jorganchem.2020.121336
0022-328X/

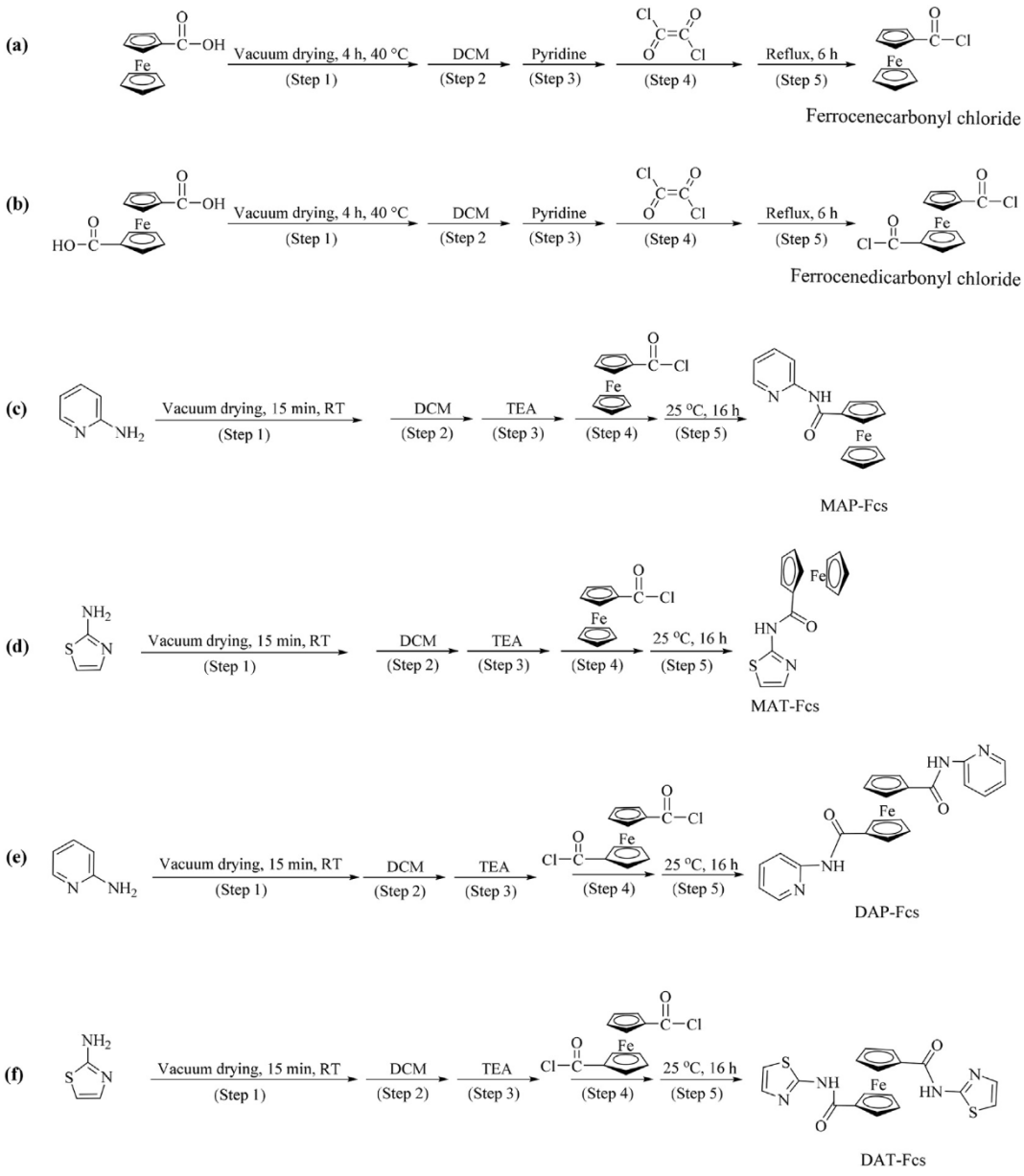

Scheme 1. Synthetic routes for (a) ferrocenecarbonyl chloride (b) ferrocenedicarbonyl chloride, (c) MAP-Fc, (d) MAT-Fc, (e) DAP-Fc and (f) DAT-Fc.

alkyl-substituted ferrocenes. TBF, NBF and catocene display excellent catalytic performances during the combustion of solid propellants. However due their shorter carbon chains on the ferrocenyl ring and lower molecular weights [46], TBF, NBF and catocene present unavoidable drawbacks such as high migratory tendency on prolonged storage, significant evaporation and sublimation loss during curing process of the propellants and phase separation by crystallization [47]. These drawbacks lead to uneven combustion, poor aging, formation of highly sensitive boundary layers and irreproducible properties of the solid propellant which reduce service life, change the designed ballistic parameters and may cause dangerous explosions [48–50]. Additionally, high electrostatic sensitivity during the mixing process of the ferrocene-based BRCs with ultra-fine AP could cause serious safety issues [51,52]. Therefore, it is necessary to overcome these migration issues and develop ferrocene-based BRCs with competent anti-migration

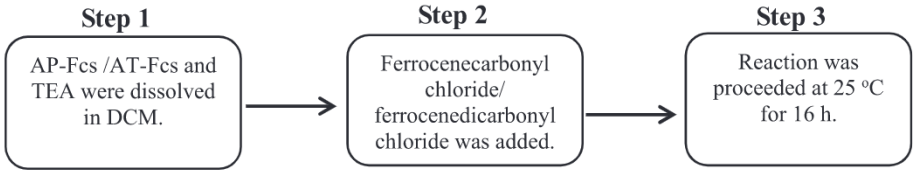

Scheme 2. Stepwise procedure for the synthesis of AP-Fcs and AT-Fcs.

Table 1
Synthetic details for the synthesis of ferrocenedicarbonyl chloride.

Compound	Step 1						Step 2			Mole ratio	Step 3	
	Acid (A)			Pyridine		DCM	Oxalyl chloride (B)				Time	Temperature
	g	mmol	$mol.L^{-1}$	mL	mmol	mL	mL	mmol	$mol.L^{-1}$	A: B	h	°C
Ferrocenecarbonyl chloride	30.0983	121.904	0.13	23	285.505	270	24	279.839	0.33	1:2.3	6	reflux
Ferrocenedicarbonyl chloride	25.2514	92.142	0.61	32	397.229	150	39	454.739	3.03	1:4.9	6	reflux

Table 2
Experimental detail for the synthesis of AP-Fcs and AT-Fcs.

Compound	Step 1						Step 2			Mole ratio	Step 3	
	Amine (A)			TEA		DCM	Ferrocenecarbonyl chloride/Ferrocenedicarbonyl chloride (B)				Time	Temperature
	g	mmol	$mol.L^{-1}$	mL	mmol	mL	g	mmol	$mol.L^{-1}$	A: B	h	°C
MAP-Fc	0.8721	9.285	0.13	1.6	11.742	70	3.0000[a]	12.072	0.17	1:1.3	16	25
MAT-Fc	0.9315	9.301	0.13	1.6	11.742	70	3.0000[a]	12.072	0.17	1:1.3	16	25
DAP-Fc	2.2250	23.643	0.33	3.0	21.697	70	3.5000[b]	11.256	0.16	1:0.47	16	25
DAT-Fc	2.3678	23.643	0.33	3.0	21.697	70	3.5000[b]	11.256	0.16	1:0.47	16	25

[a] Ferrocenecarbonyl chloride (g).
[b] Ferrocenedicarbonyl chloride (g).

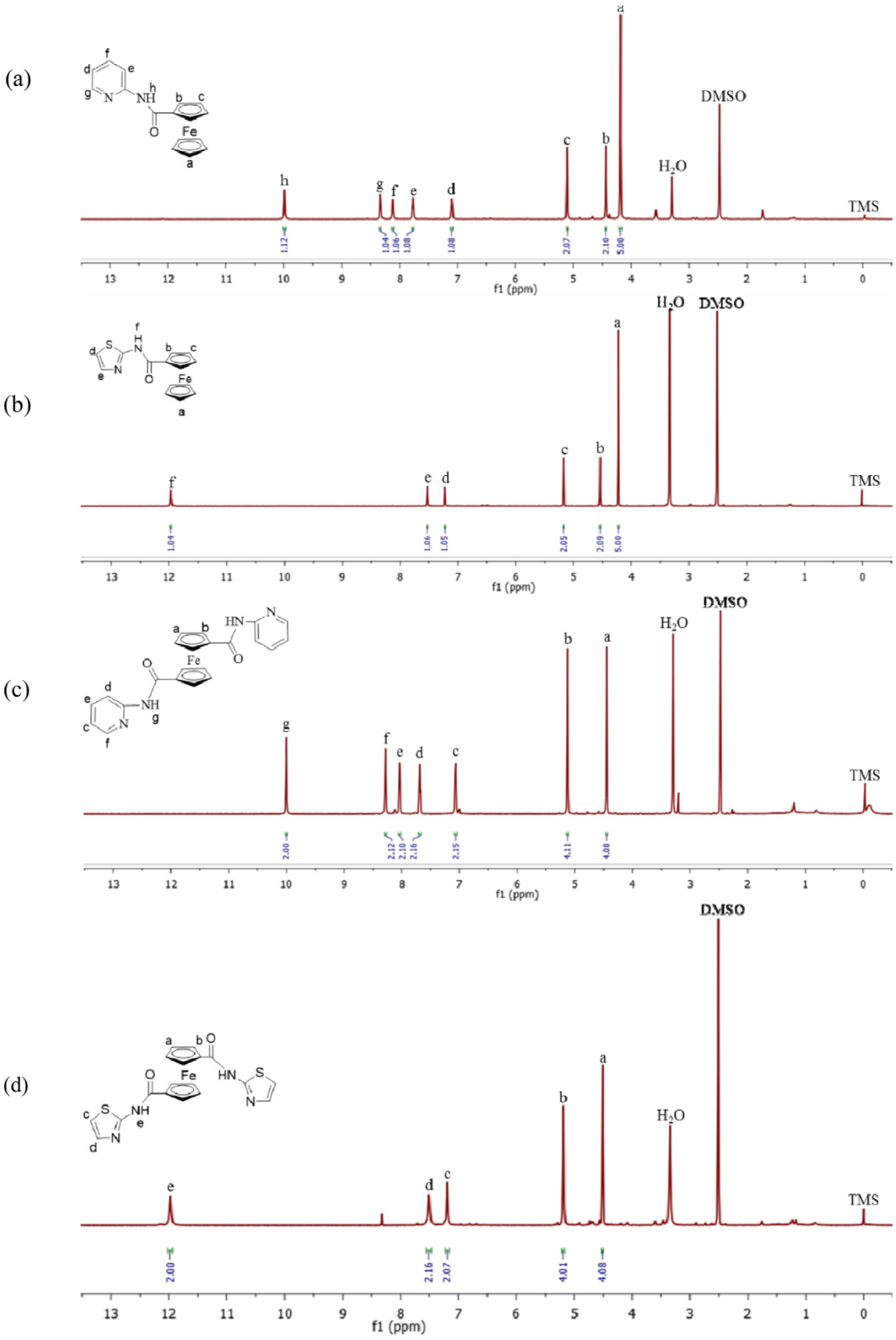

Fig. 1. ^{1}H NMR spectra of (a) MAP-Fc, (b) MAT-Fc, (c) DAP-Fc and (d) DAT-Fc.

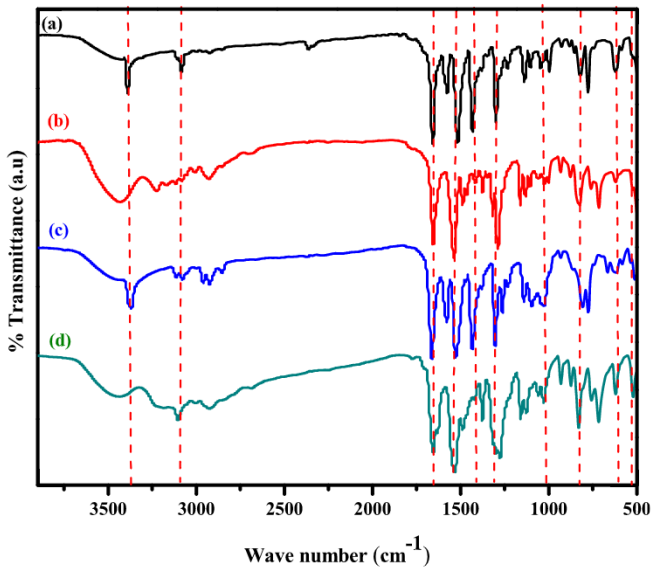

Fig. 2. FT-IR spectra of (a) MAP-Fc, (b) MAT-Fc, (c) DAP-Fc and (d) DAT-Fc.

features and enhanced burning rate catalytic performances [53–55]. Since the BR catalytic performance depends on chemical structure, solubility and iron content of ferrocene derivatives [52], various researchers have synthesized different ferrocene-based BRCs. Recently, ferrocene-contained heterocyclic compounds have gained considerable interest because of their unique properties [56,57]. Ferrocenylated compounds with nitrogen-rich heterocyclic rings have been less explored as BRCs in solid propellants. Such compounds showed good catalytic efficiency in solid propellants [15,46,50].

Herein, we will synthesize ferrocene-based aminopyridines (AP-Fcs) and ferrocene-based aminothiazoles (AT-Fcs) as BRCs. AP-Fcs contain ferrocenylated monoaminopyridine (MAP-Fc) and ferrocenylated diaminopyridine (DAP-Fc), while AT-Fcs include ferrocenylated monoaminothiazole (MAT-Fc) and ferrocenylated diaminothiazole (DAT-Fc). The core reason of choosing AP-Fcs and AT-Fcs is ferrocene derivatives could be used as potential BRCs in composite solid propellants and the presence of nitrogen rich heterocyclic rings (with high energy C-N bonds) can contribute energy to the propellants [58].

2. Experimental section

2.1. Materials

2-aminopyridine (AMP) and 2-aminothiazole (AMT) were purchased from J&K Co. Ltd. Oxalyl chloride, dichloromethane (DCM), petroleum ether, pyridine, chloroform ($CHCl_3$), and triethylamine (TEA) were purchased from Sinopharm Co. Ltd. Hydroxyl-terminated polybutadiene (HTPB) ferrocenecarboxylic acid, ferrocenedicarboxylic acid, isophorone diisocyanate, sodium bicarbonate ($NaHCO_3$) and tetrabutylammonium tetrafluoroborate (Bu_4NBF_4) was purchased from Aladdin chemicals Co. Ltd. Before use, DCM and TEA were distilled over calcium hydride. Pyridine and petroleum ether were dried with 4A-type molecular sieves. Other chemicals were used as received.

Table 3
FT-IR data of AP-Fcs and AT-Fcs.

AP-Fcs and AT-Fcs				Band assignment [8,22,36,60–68]
MAP-Fc	MAT-Fc	DAP-Fc	DAT-Fc	
3391	3420	3370	3425	NH- str.
3103	3103	3098	3099	C-H str. of Cp rings
3076	3082	3078	3103	C-H str.
1660	1665	1648	1660	C=N str.
1290	1285	1306	1279	C-N str.
1527	1534	1529	1539	C=C str.
–	617	–	618	C-S str.
1431	–	1430	–	C-C bend.
503	497	508	505	Cp-Fe str.

Table 4
Detail of samples preparation for CV studies.

Compound	Amount of sample			Amount of electrolyte (Bu_4NBF_4)			Solvent	Volume of solution
	g	mmol	$mol.L^{-1}$	g	mmol	$mol.L^{-1}$		mL
MAP-Fc	0.0021	0.01	0.69	0.3367	1.02	102	DCM	10
MAT-Fc	0.0023	0.01	0.74	0.3341	1.01	101	DCM	10
DAP-Fc	0.0032	0.01	0.72	0.3310	1.01	101	DCM	10
DAT-Fc	0.0032	0.01	0.70	0.3324	1.01	101	DCM	10

Table 5
Detail of samples preparation for CV studies.

Compound	Amount of sample			Amount of electrolyte (Bu_4NBF_4)			Solvent	Volume of solution
	g	mmol	$mol.L^{-1}$	g	mmol	$mol.L^{1}$		mL
MAP-Fc	0.0024	0.01	0.78	0.3301	1.00	100	$CHCl_3$	10
MAT-Fc	0.0030	0.01	0.96	0.3298	1.00	100	$CHCl_3$	10
DAP-Fc	0.0026	0.01	0.59	0.3362	1.02	102	$CHCl_3$	10
DAT-Fc	0.0029	0.01	0.64	0.3377	1.03	103	$CHCl_3$	10

Table 6
Detail of samples preparation for CV studies.

Compound	Amount of sample			Amount of electrolyte (Bu_4NBF_4)			Solvent	Volume of solution
	g	mmol	$mol.L^{-1}$	g	mmol	$mol.L^{-1}$		mL
MAP-Fc	0.0024	0.01	0.78	0.3366	1.02	100	DMSO	10
MAT-Fc	0.0023	0.01	0.74	0.3299	1.00	100	DMSO	10
DAP-Fc	0.0027	0.01	0.61	0.3306	1.00	100	DMSO	10
DAT-Fc	0.0026	0.01	0.57	0.3356	1.02	102	DMSO	10

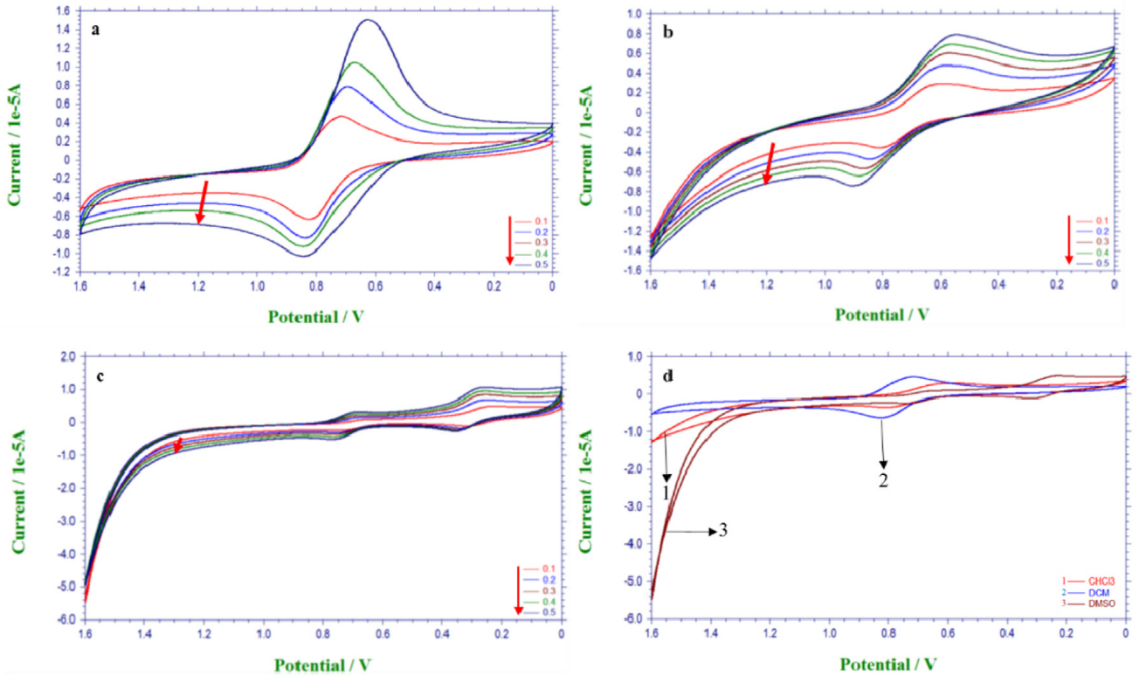

Fig. 3. CV curves of MAP-Fc in: (a) DCM, (b) $CHCl_3$, (c) DMSO at different potential scan rates (d) different organic solvents: (1) $CHCl_3$, (2) DCM and (3) DMSO at 0.1 V/s.

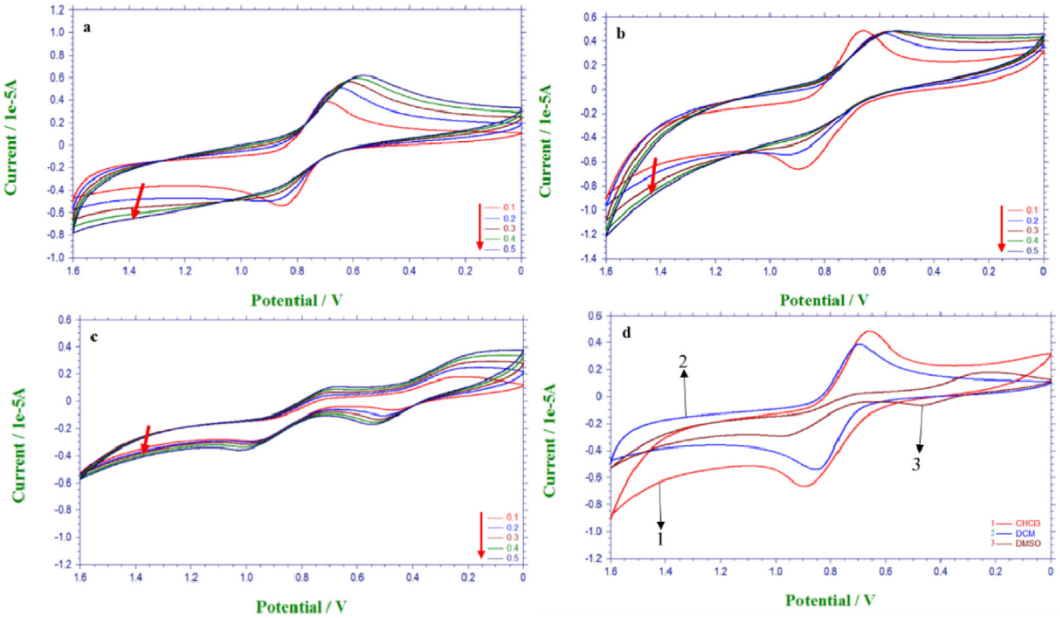

Fig. 4. CV curves of MAT-Fc in: (a) DCM, (b) $CHCl_3$, (c) DMSO at different potential scan rates and (d) different organic solvents: (1) $CHCl_3$, (2) DCM and (3) DMSO at 0.1 V/s.

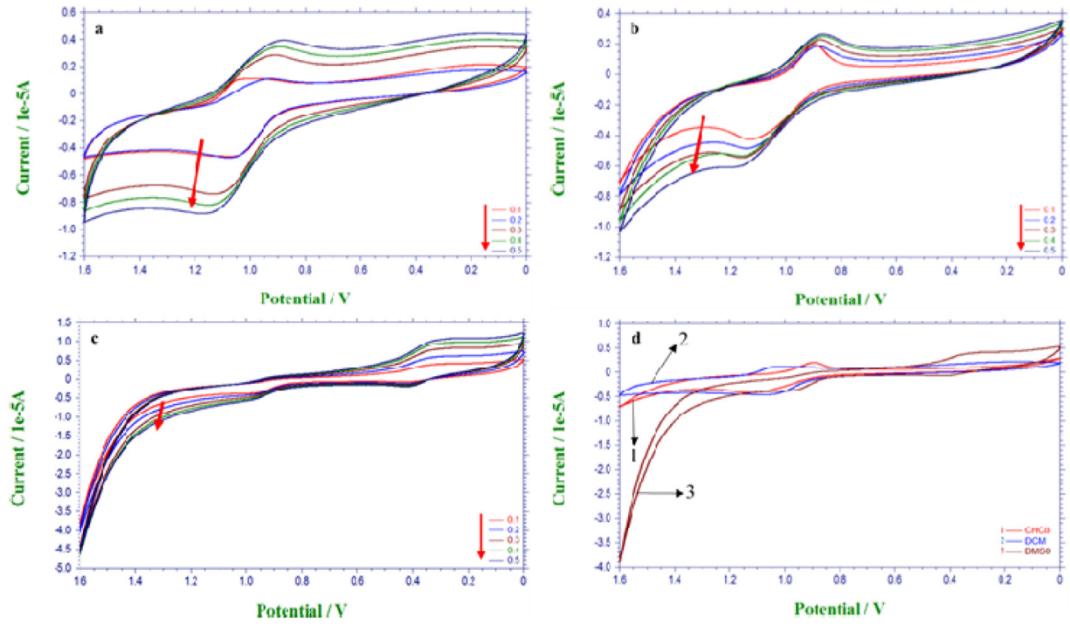

Fig. 5. CV curves of DAP-Fc in: (a) DCM, (b) $CHCl_3$, (c) DMSO at different potential scan rates and (d) different organic solvents: (1) $CHCl_3$, (2) DCM and (3) DMSO at 0.1 V/s.

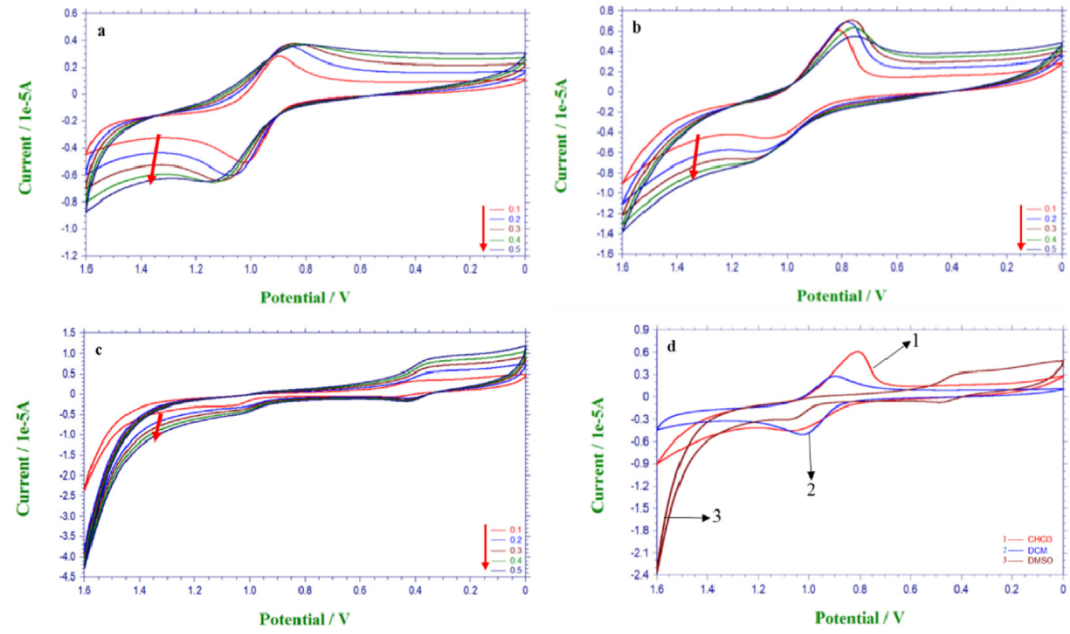

Fig. 6. CV curves of DAT-Fc in: (a) DCM, (b) $CHCl_3$, (c) DMSO at different potential scan rates and (d) different organic solvents: (1) $CHCl_3$, (2) DCM and (3) DMSO at 0.1 V/s.

2.2. Synthesis

2.2.1. Synthesis of ferrocenecarbonyl chloride

Synthesis of ferrocenecarbonyl chloride was carried out by following a previously reported method [59]. At first ferrocenecarboxylic acid (30.0972 g, 121.899 mmol) was dried under reduced. Afterward, freshly distilled DCM (170 mL) was injected to dried ferrocenecarboxylic acid to make ferrocenecarboxylic acid solution. Pyridine (22 mL, 273.123 mmol) was then injected into the resulting ferrocenecarboxylic acid solution. The obtained mixture was stirred at room temperature for 15 min under argon atmosphere. Subsequently, at room temperature oxalyl chloride (23 mL, 268.179 mmol) was injected slowly to the previous mixture. The acquired reaction mixture was then refluxed for 5 h. The solvent was evaporated under reduced pressure and ferrocenecarbonyl chloride was extracted using petroleum ether (150 mL) at 90 °C. Ferrocenecarbonyl chloride was kept in Ar atmosphere for further use [59].

2.3. Synthesis of ferrocenedicarbonyl chloride

Ferrocenedicarbonyl chloride was synthesized with modifications to the previously reported method [60]. Ferrocenedicarboxylic acid (25.2514 g, 92.142 mmol) was taken into a two neck-flask.

Table 7
Electrochemical data of AP-Fcs and AT-Fcs in different organic solvents at 0.1 V/s.

Compound	Solvent	E_{Pc} (mV)	E_{Pa} (mV)	$^{a}E_{P}^{1/2}$ (mV)	$^{b}\Delta E_{P}$ (mV)	i_{pc} (μA)	i_{pa} (μA)	i_{pa}/i_{pc}
MAP-Fc	DCM	716	825	771	109	5.11E-03	4.68E-03	0.915
	$CHCl_3$	601	812	707	211	2.14E-03	2.15E-03	1.005
	DMSO	226	319	273	93	2.37E-03	1.85E-03	0.781
MAT-Fc	DCM	695	856	776	161	3.95E-03	4.10E-03	1.038
	$CHCl_3$	658	889	774	231	4.63E-03	6.68E-03	1.444
	DMSO	242	473	358	231	1.78E-03	2.49E-03	24.536
DAP-Fc	DCM	948	1076	1012	128	1.12 E−03	2.49E-03	2.237
	$CHCl_3$	896	1128	1012	232	1.95 E−03	4.30E-03	2.212
	DMSO	333	424	378	91	3.96E-03	3.27E-03	0.826
DAT-Fc	DCM	897	1026	962	129	2.96E-03	3.83E-03	1.292
	$CHCl_3$	810	1057	934	247	4.56E-03	4.06E-03	0.891
	DMSO	351	430	391	79	3.62E-03	5.37E-03	0.148

Table 8
Detail of samples preparation for anti-migration studies.

Sample	Ammonium perchlorate		Burning rate catalyst		Hydroxyl-terminated polybutadiene		Isophorone diisocyanate	
	g	Wt. %	g	Wt. %	g	Wt. %	g	Wt. %
MAP-Fc	2.2591	67.44	0.0599	1.79	0.6617	19.75	0.3692	11.02
MAT-Fc	2.4563	68.53	0.0516	1.44	0.6791	19.95	0.3973	11.08
DAP-Fc	2.3059	67.36	0.0518	1.51	0.6791	19.84	0.3863	11.29
DAT-Fc	2.2141	67.69	0.0536	1.64	0.6568	20.08	0.3462	10.58
Catocene	2.2537	75.65	0.0599	2.01	0.6654	22.34	0.3069	9.43
Ferrocene	2.2585	68.66	0.0551	1.68	0.6745	20.51	0.3009	9.15
Blank	13.4745	77.36			3.9318	2.57	1.7991	10.33

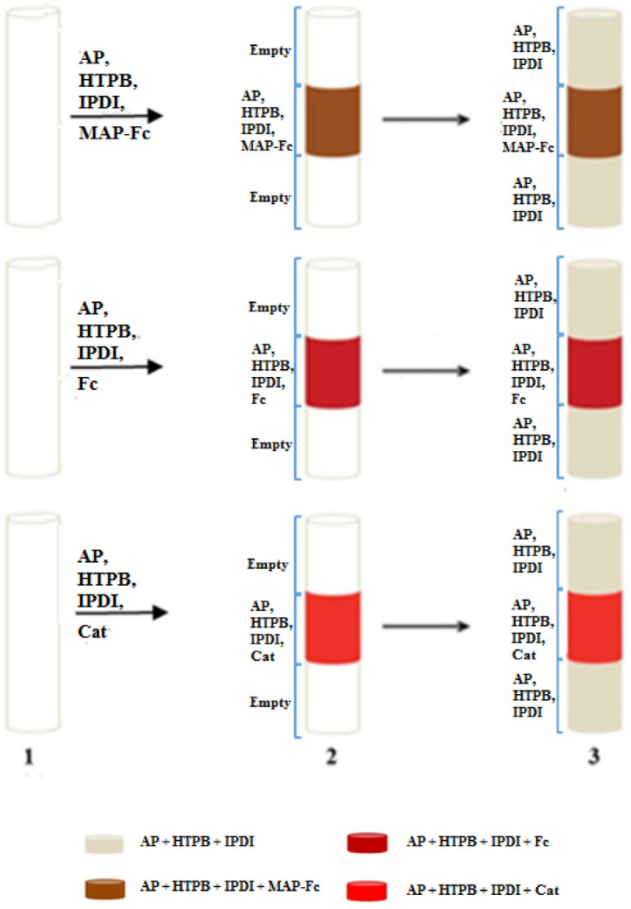

Fig. 7. Schematic procedure for the fabrication of migration tubes: (1) empty tube, (2) tube filled with loaded part and (3) tube filled with loaded and unloaded part.

Ferrocenedicarboxylic acid was dried and dissolved in freshly distilled DCM (150 mL) to prepare ferrocenedicarboxylic acid solution. Pyridine (32 mL, 397.229 mmol) was injected to ferrocenedicarboxylic acid solution and the resultant mixture was allowed to stir for 15 min. Later, oxalyl chloride (39 mL, 454.739 mmol) was put slowly to the resulting mixture. The obtained reactant mixture was then refluxed for 6 h. As the reaction was completed, the solvent in the reaction flask was evaporated and the product (ferrocenedicarbonyl chloride) was extracted with petroleum ether (150 mL) at 90 °C.

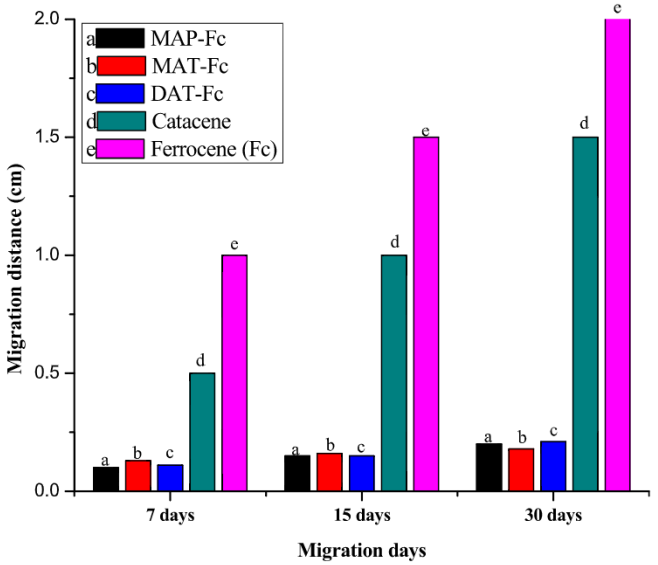

Fig. 8. Anti-migration studies of (a) MAP-Fc, (b) MAT-Fc, (c) DAT-Fc, (d) catocene and (e) ferrocene on days 7, 15 and 30 at 50 °C.

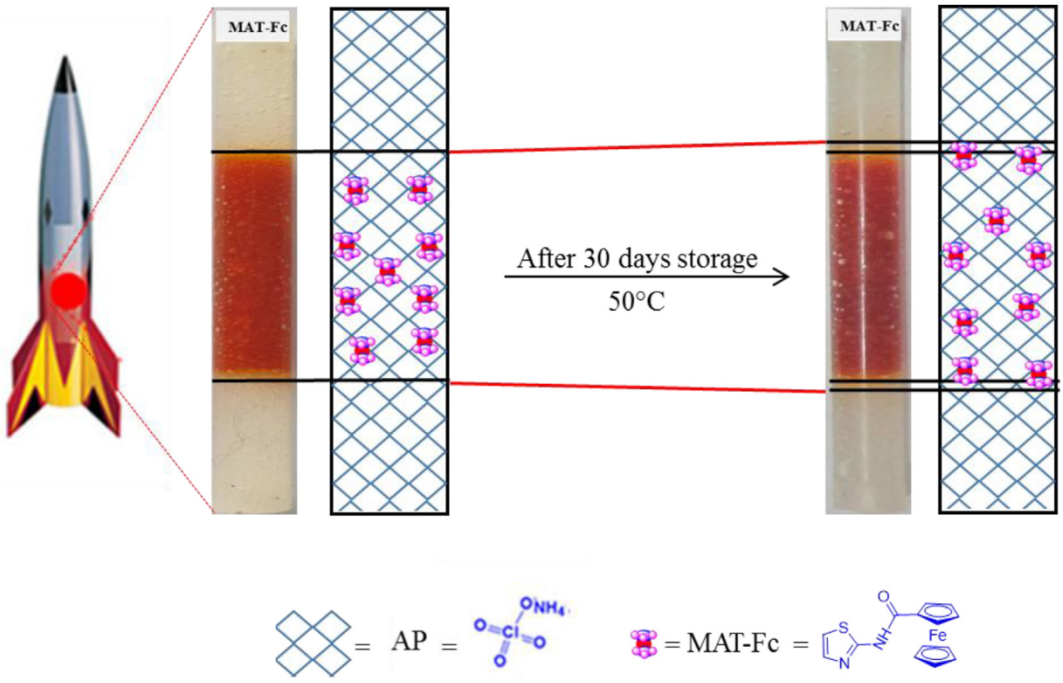

Fig. 9. Anti-migration mechanism of MAT-Fc.

2.3.1. Synthesis of ferrocene-based aminopyridines (AP-Fcs) and aminothiazoles (AT-Fcs)

The synthetic route of AP-Fcs comprised of condensation reactions between aminopyridine and ferrocenecarbonyl chlorides. Similarly, AT-Fcs were synthesized by reacting aminothiazole with ferrocenecarbonyl chlorides [60,61] Synthesis of ferrocenylated monoaminopyridine (MAP-Fc) is taken as an example. To synthesize MAP-Fc, aminopyridine (0.8721 g, 9.285 mmol) was taken into a two-neck flask. Aminopyridine was dried and then dissolved in freshly distilled DCM (35 mL) to get aminopyridine solution. Afterward, TEA (1.6 mL, 11.742 mmol) was added to aminopyridine solution. Later on, ferrocenecarbonyl chloride (3.0000 g, 12.072 mmol) was added slowly to the reaction mixture. The reaction mixture was then kept at constant stirring for 16 h at 25 °C. When the reaction was finished the solvent was removed using rotary dryer to get crude MAP-Fc. The get pure MAP-Fc, crude MAP-Fc was added to $CHCl_3$ (200 mL) to form its solution. Then the crude MAP-Fc solution was washed with 1% $NaHCO_3$ solution and distilled water, respectively. Afterward, the solution was separated to obtain the organic layer. To the organic layer anhydrous Na_2SO_4 was added and the resultant mixture was stored overnight. Later, the mixture was filtered and dried to obtain pure MAP-Fc. MAP-Fc was placed in vacuum oven for complete dryness (till constant weight). To synthesize ferrocenylated monoaminothiazole (MAT-Fc), ferrocenylated diaminopyridine (DAP-Fc) and ferrocenylated diaminothiazole (DAT-Fc), similar synthetic procedure (*i.e.* mentioned above) was used.

2.4. Characterization

^{1}H NMR spectra were obtained using AVANCE NMR spectrometer (600 MHz, model DMX-400). For CV investigations CHI-630A electrochemical analyzer (CH Instruments Inc., Austin, TX) was used. For every CV analysis electrolyte (Bu_4NBF_4) concentration of 0.1 M and 0.5 mM concentration of ferrocene compounds was used. The potential scan rate range of 0.1–0.5 V^{-1} was used for each CV experiment. The anti-migration studies of (AP-Fcs) and (AT-Fcs) was carried out using migration tubes. The tubes for anti-migration performances were prepared in accordance to previously reported literature. The migration tube consisted of: a loaded segment, an interface and an unloaded portion. The loaded segment was composed of AP, HTPB, IPDI and a BRC. AP, HTPB, IPDI and BRC was mixed together to get a homogeneous gel. The resulting gel was well packed into a glass tube and then cured at room temperature for 72 h. The unloaded portion contained AP, HTPB and IPDI. AP, HTPB and IPDI were mixed together to obtain whitish sludge like mixture, which was cast on the cured loaded part in the glass tube. The BR catalytic performances of (AP-Fcs) and (AT-Fcs) were explored using TA Q500 thermogravimetric analyzer with heating at 10 °C min^{-1} and for temperature range of 50–600 °C.

3. Results and discussions

3.1. Synthesis and characterization

Ferrocenecarbonyl chloride and ferrocenedicarbonyl chloride were prepared in accordance to the reported methods [61]. The synthetic schemes of ferrocenecarbonyl chlorides, AP-Fcs (MAP-Fc and DAP-Fc) and AT-Fcs (MAT-Fc and DAT-Fc) is shown in Scheme 1(a-f). Stepwise procedure for the synthesis of AP-Fcs and AT-Fcs is given in Scheme 2.

The experimental synthetic details of ferrocenecarbonyl chloride and ferrocenedicarbonyl chloride is given in Table 1 while experimental synthetic details of AP-Fcs and AT-Fcs are given in Table 2.

The structures of AP-Fcs and AT-Fcs were characterized by ^{1}H NMR and FT-IR. The appearance of new peaks (at 4.00–5.00 ppm) attributed to ferrocene protons [62,63]. ^{1}H NMR spectra of AP-Fcs and AT-Fcs are shown by Fig. 1(a-d).

The chemical shift data for MAP-Fc was: δ (ppm) = 4.19(5H, H_a), 4.44(2H, H_b), 5.11(2H, H_c), 7.10(1H, H_d), 7.77(1H, H_e), 8.11(1H, H_f), 8.33(1H, H_g), 9.99(1H, H_h).

For MAT-Fc the data of chemical shift was: δ (ppm) = 4.22(5H, H_a), 4.54(2H, H_b), 5.17(2H, H_c), 7.22(1H, H_d), 7.53(1H, H_e), 11.97(1H, H_f).

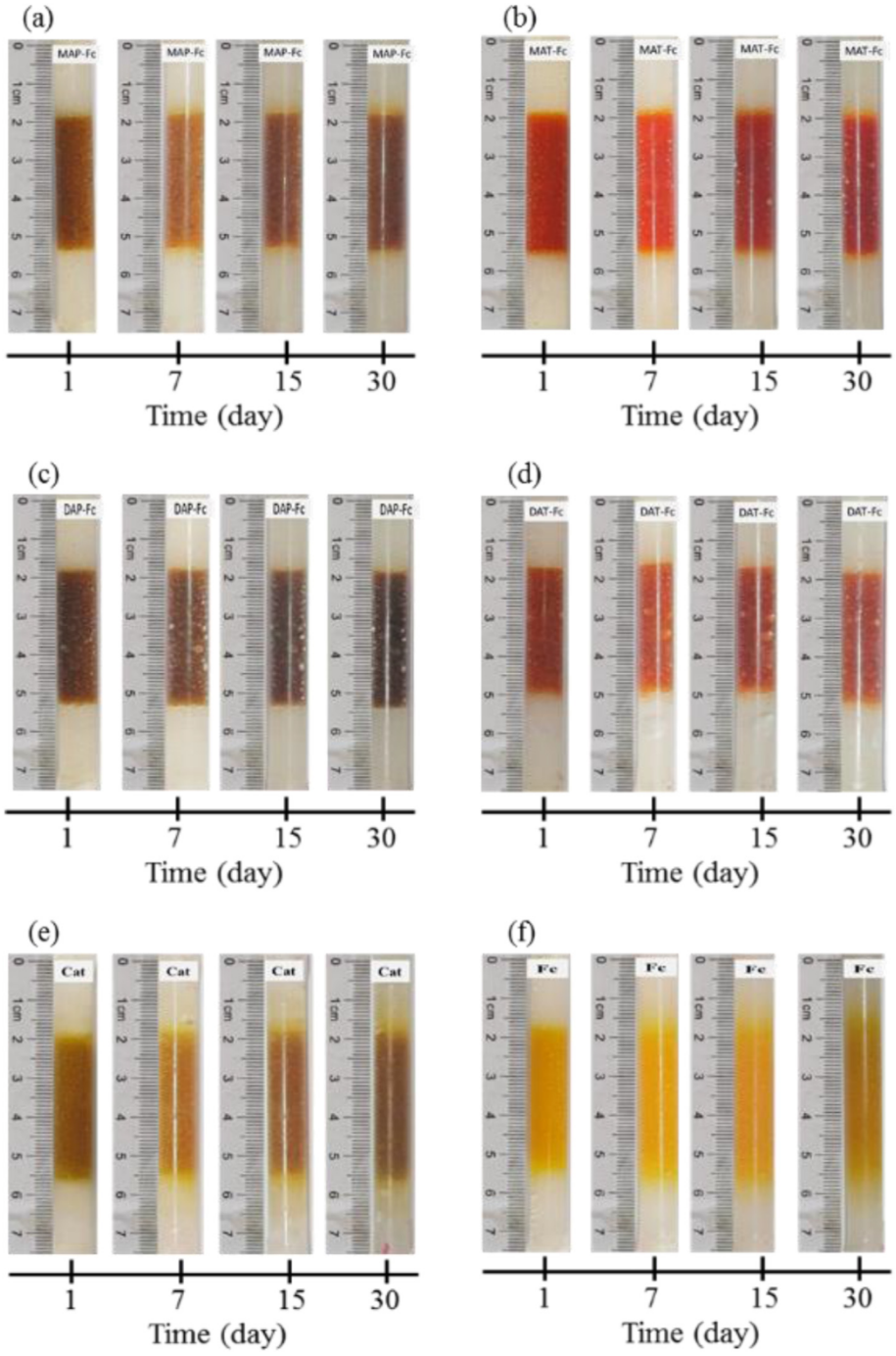

Fig. 10. Anti-migration studies photos of: (a) MAP-Fc, (b) MAT-Fc, (c) DAP-Fc, (d) DAT-Fc, (e) catocene and (f) ferrocene on days 1, 7, 15 and 30 at 50 °C.

The chemical shift data for DAP-Fc was found as: δ (ppm) = 4.45(4H, H_a), 5.12(4H, H_b), 7.06(2H, H_c), 7.76(2H, H_d), 8.04(2H, H_e), 8.28(2H, H_f), 10.00(2H, H_g).

In the case of DAT-Fc, the chemical shift data was noted as: δ (ppm) = 4.51(4H, H_a), 5.18(4H, H_b), 7.19(2H, H_c), 7.50(2H, H_d), 11.97(2H, H_e).

The ferrocenylated compounds were further characterized with FT-IR spectroscopy. FTIR results for AP-Fcs and AT-Fcs indicated their successful synthesis. The vibrational and deformational bands of ferrocenyl unit were evident at 1015–1045 cm^{-1}, 801–835 cm^{-1} and 497–505 cm^{-1} [8,22]. The absorption peak between 3350 and 3450 cm^{-1} are assigned to stretching vibrations of secondary NH–groups [64,65]. The C=N stretching (str.) appeared as a strong band at around 1650 cm^{-1} [65–67]. The bands observed around 1530 cm^{-1} are attributed to C=C stretching vibrations [68] whereas the absorption bands between 1270 cm^{-1}–1310 cm^{-1} are attributed to C-N stretching vibrations [69]. The bands around 620 cm^{-1} in spectra of MAT-Fc and DAT-Fc are linked with the C-S stretching vibration [70] while the peaks at 1430 cm^{-1} in MAP-Fc and DAP-Fc are attributed to C-C stretching vibrations [71]. The C-H stretching vibrations are noticed to be located in the range of 3000–3100 cm^{-1} [72,73]. FT-IR spectra of AP-Fcs and AT-Fcs is shown by Fig. 2. Table 3 presents the different band assignments for the functional groups.

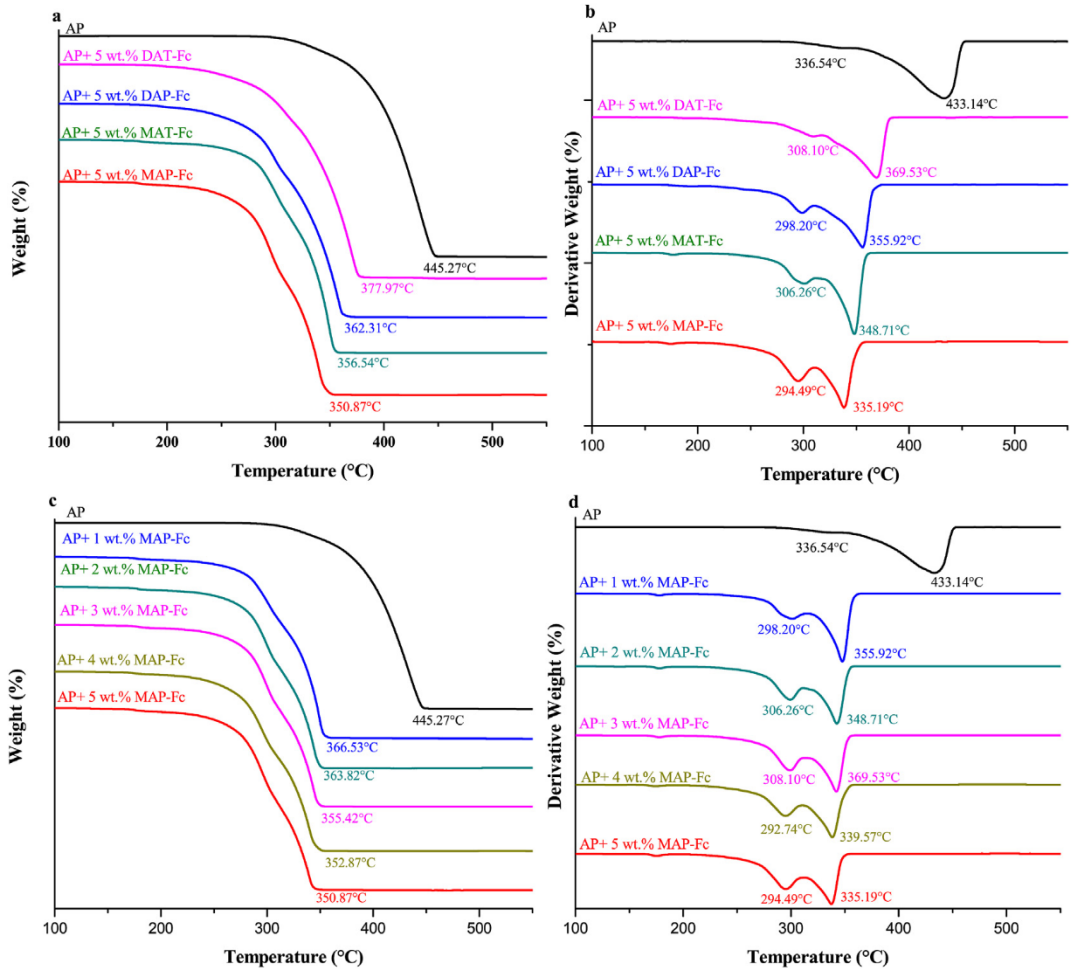

Fig. 11. (a) TG curves of pure AP and AP with 5 wt% of AP-Fcs and AT-Fcs, (b) DTG curves of pure AP and AP with 5 wt% of AP-Fcs and AT-Fcs, (c) TG curves of pure AP and AP with 1–5 wt% of MAP-Fc and (d) DTG curves of pure AP and AP with 1–5 wt% of MAP-Fc.

Table 9
Samples preparation for TG and DTG analysis.

Compound	Sample code	Amount of compound (mg)	Amount of AP (mg)	Total amount (mg)	Wt.% of the compound (%)	Amount of sample used (mg)
MAP-Fc	AP + 5 wt% MAP-Fc	1.4	26.8	28.2	5.0	3.01
MAT-Fc	AP + 5 wt% MAT-Fc	1.6	31.5	33.1	5.0	3.21
DAP-Fc	AP + 5 wt% DAP-Fc	1.9	36.7	38.6	5.0	2.87
DAT-Fc	AP + 5 wt% DAT-Fc	1.5	28.6	30.1	5.0	3.30

3.2. Electrochemical behavior

Electrochemical reaction mechanism of ferrocene-based BRCs is linked with its combustion catalytic performance in composite solid propellants [9,50,58]. As proposed in the combustion catalytic mechanism of ferrocene-based BRCs, the electron transfer between Fe^{2+} and Fe^{3+}ions in the ferrocenyl groups through oxidation by AP and reduction by NH_3 (produced by the thermal decomposition of AP) was involved in the enhancement of the decomposition reaction rate below 300 °C [21,47,74,75]. Hence it necessary to investigate the redox properties of ferrocene-based BRCs to deepen and broaden our insight into the catalytic mechanism of the BRCs [76]. CV is an effective method for exploring the electrochemistry of ferrocene and its derivatives [77]. Ferrocenyl derivatives present different electrochemical behaviors in different solvents. Therefore, the electrochemical properties of AP-Fcs and AT-Fcs were evaluated using DCM, $CHCl_3$ and DMSO. CV results indicated that AP-Fcs and AT-Fcs showed different redox behaviors in different solvents. The change in redox behavior was attributed to the polarity of solvents and potential scan rate [3,78–82]. The sample preparation details is given in Tables 4–6.

The solvents influenced the shape of the CV curves due to variation of solvent polarity. The increase of solvent polarity caused deformation of the peak shapes and decrease of the peak currents [83]. The CV curves of AP-Fcs and AT-Fcs were deformed in DMSO. The increase of polarity lead to decrease of both the oxidation and reduction peaks potential. The decrease in oxidation and reduction peaks potential indicated that reduction and oxidation processes of AP-Fcs and AT-Fcs were in direct proportion to the solvent polarity [62,63]. In DCM and $CHCl_3$ more expanded and sharp peaks were obtained. The maximum peak-to-peak potential separation (ΔE_p) was found in $CHCl_3$ whereas the lowest ΔE_p values were observed in DMSO. In case of DCM and $CHCl_3$, AP-Fcs and AT-Fcs showed single redox peak whereas in DMSO two redox peaks were

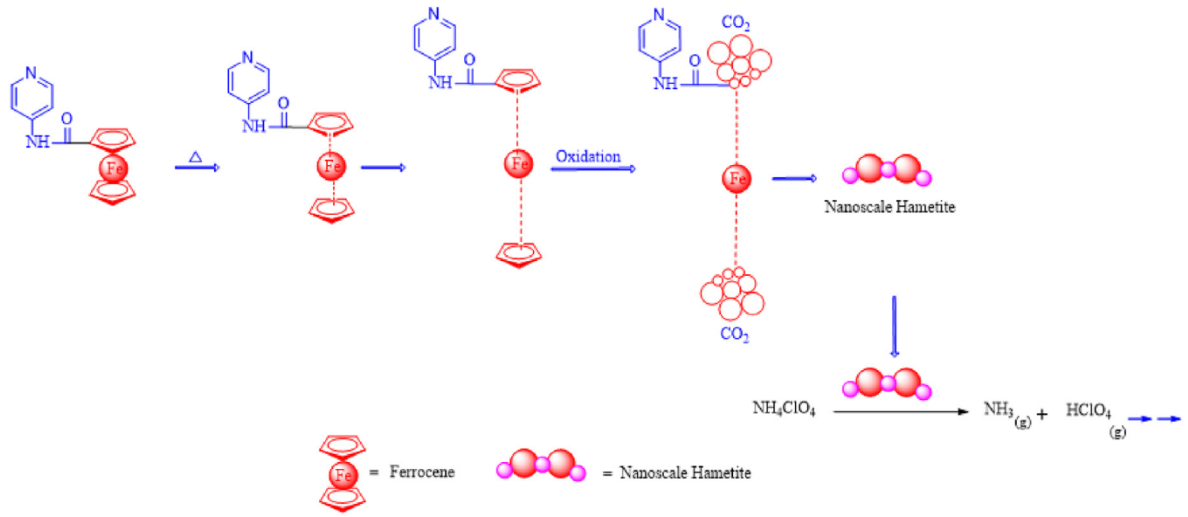

Fig. 12. The possible BR catalytic mechanism for thermal decomposition of AP catalyzed by MAP-Fcs and AT-Fcs.

emerged. The emergence of two redox peaks in DMSO might be due to high viscosity of DMSO and interactions of AP-Fcs and AT-Fcs with DMSO. In DCM and $CHCl_3$ the single redox peak indicated that all ferrocene units acted in similar manner. In a solvent with higher polarity, the oxidized states of AP-Fcs and AT-Fcs were more stable andwas harder to reduce.

The electrochemical properties of AP-Fcs and AT-Fcs was also examined at different potential scan rates. CV curves of AP-Fcs and AT-Fcs at different potential scan rates (0.1 V/s −0.5 V/s) and in different organic solvents are shown in Figs. 3–6. Electrochemical data of AP-Fcs and AT-Fcs in different organic solvents at 0.1 V/s is shown by Table 7.

AP-Fcs and AT-Fcs were found sensitive to the potential scan rate and it was noticed that the peak currents (i_{pa} and i_{pc}) were increased with high potential scan rate. From The CV results showed that charge transport of the electrode processes followed Fick's law at room temperature and the electrode processes were diffusion controlled [84]. The electrode reaction was faster in DCM. Furthermore, the charge diffusion rate of DCM was faster because of its less resistance [78]. The easy the charge transfer between the active sites facilitated distinct oxidation and reduction peaks of AP-Fcs and AT-Fcs in CV studies and it can be concluded AP-Fcs and AT-Fcs presented such electrochemical processes that were neither completely reversible nor fully irreversible [84].

3.3. Anti-migration behavior

AP-Fcs and AT-Fcs were tested for anti-migration performances against ferrocene and catocene for a time period of 30 days at 50 °C. The sample preparation for the anti-migration tests is given in Table 8. The migration tube fabrication process is illustrated in Fig. 7.

AP-Fcs and AT-Fcs showed anti-migratory behavior in comparison to ferrocene as well as catocene. AP-Fcs and AT-Fcs contained N-H groups within their structure which lead to good anti-migration performances. The N-H groups resulted in formation of hydrogen bond and dipole−dipole interactions. The stronger attractive forces bonded the ferrocenylated compounds and propellant together and hence retarded the migratory tendency within the propellant. Anti-migration performances of MAP-Fc, MAT-Fc, DAP-Fc and DAT-Fc, catocene as well as ferrocene are shown in Fig. 8 and anti-migration mechanism of MAT-Fc is shown in Fig. 9. Anti-migration studies photos of MAP-Fc, MAT-Fc, DAP-Fc, DAT-Fc, catocene and ferrocene are shown in Fig. 10.

3.4. Burning rate catalytic effect and catalytic mechanism

Thermally stable BRCs are regarded significant, as they are anticipated to facilitate the smooth burning of the propellants [50]. AP accounts for 60–90% of the composite solid propellant, therefore its thermal decomposition is believed to greatly influence the burning velocity and combustion of propellants. In AP-based propellants, thermal decomposition of AP predominantly affects the propellant performance. Therefore the BR catalytic effect of a ferrocene-based BRC is generally verified by exploring its catalytic effect on the thermal decomposition of AP.

The BR catalytic performances of AP-Fcs and AT-Fcs of AP was evaluated using TG and DTG techniques.5 wt % mixture of the ferrocenylated compounds with AP was chosen for conduct of the thermal analysis.

Fig. 11(a) and Fig. 11(b) illustrates thermogravimetric results for pure AP and its mixtures with AP-Fcs and AT-Fcs. The BR catalytic performance of MAP-Fc was also analyzed by using its different weight content (1–5 wt.%). Fig. 11(c) and 11(d) shows the TG and DTG results of MAP-Fc at its different weight content for the thermal decomposition of AP. Table 9 highlights the details of samples used for thermogravimetric studies. The TG and DTG figures indicated that AP-Fcs and AT-Fcs provided catalytic effect and they promoted the thermal decomposition of AP. The addition of AP-Fcs and AT-Fcs as an additive contributed towards the fast decomposition of AP. In TG studies the thermal decomposition temperature of AP was found to be at 445.27 °C, but after adding AP-Fcs and AT-Fcs (5 wt%) to AP, the decomposition temperature for AP decreased up to 350.87 °C. The addition of AP-Fcs and AT-Fcs clearly affected decomposition temperature of AP as it shifted the decomposition peaks towards the left, which is indicative of lower decomposition temperature values. AP-Fcs and AT-Fcs accelerated the decomposition of AP as well as they increased the of heat content during thermal decomposition of AP [85].

Among all the ferrocene-based compounds MAP-Fc showed the highest catalytic activity (Fig. 11(a)) as it lowered the thermal disintegration temperature of AP by 94 °C. Furthermore, from Fig. 11(c) it was noticed that the high wt. % of MAP-Fc contributed towards higher catalytic activity and decreased thermal decomposition temperatures of AP. The increase in catalytic effect shown by decreasing decomposition temperatures was probably delivered by the increasing ferrocene content, which is considered to have a strong catalytic effect and promote accelerated thermal

decomposition of AP. This increase in wt. % of MAP-Fc resulted in forward (towards left) shifting of decomposition peaks (Fig. 11(d)), thereby indicated the fast thermal decomposition of AP.

In Fig. 11(b) the DTG results of pure AP and its mixtures with AP-Fcs and AT-Fcs indicated multi stage decomposition. The initial decomposition was marked as low temperature decomposition (LTD). LTD occurred at low temperature values and it involved fractional decomposition of AP.Meanwhile the second stage decompositions of AP were at observed at high temperatures. These high temperature decomposition of were referred as HTD and it involved the complete decomposition of AP. The TG curve of pure AP, indicated that LTD of pure AP was found at 336.54 °C while the HTD occurred at 433.14 °C. For AP-Fcs and AT-Fcs mixtures, the TG results showed that LTD was about 300 °C and HTD was located around 350 °C 5 wt% MAP-Fc was found to be most effective in terms maximum weight loss and with highest decrease of decomposition temperature (Fig. 11(b)). It was proven by the experimental results that the increase in wt. % of MAP-Fc, facilitated the thermal decomposition of AP at rapid rate (Fig. 11(d)). The temperature decreasing trend in both LTD and HTD proved that the AP-Fcs and AT-Fcs hold catalytic effect in lowering the thermal decomposition of AP.

The BR catalytic mechanism of ferrocene-based compounds in AP-based propellant can be described in terms of its relation to the thermal decomposition of AP [62]. The presence of ferrocene-based BRCs within the propellant promote accelerated decomposition of AP by electron transfer mechanism [49].

As combustion of composite solid propellants is a complex redox reaction, therefore it presents complications. In the combustion of AP-based propellants, it is supposed that ferrocene-based derivatives are transformed into small scale iron oxide (Fe_2O_3) particles [86]. These nano Fe_2O_3 particles have large surface area and can absorb ClO_4 in its gaseous phase to catalyze the rupture of the chemical bond in AP [8] Hence, both the electron transfer process and the catalytic decomposition effect of Fe_2O_3 particles can significantly contribute towards the thermal decomposition of AP. Based on references, the larger surface area of nano Fe_2O_3 particles offers high catalytic effect and exhibit excellent BR catalytic effect in thermal decomposition of AP [49,53,86–88]. The possible BR catalytic mechanism for thermal decomposition of AP catalyzed by AP-Fcs and AT-Fcs is illustrated by Fig. 12.

4. Conclusion

AP-Fcs and AT-Fcs have been synthesized as BRCS. AP-Fcs and AT-Fcs were characterized by ^{1}H NMR and FT-IR spectroscopy. The electrochemical behavior of AP-Fcs and AT-Fcs were analyzed by CV in different organic solvents and at different potential scan rates. AP-Fcs and AT-Fcs were analyzed for anti-migration properties in comparison with catocene and ferrocene. AP-Fcs and AT-Fcs were analyzed for their BR catalytic performances on thermal decomposition of AP.

^{1}H NMR and FT-IR spectra confirmed the synthesis of AP-Fcs and AT-Fcs. The electrochemical investigations showed that oxidation and reduction reaction of AP-Fcs and AT-Fcs were diffusion controlled. The thermogravimetric results confirmed high BR catalytic activities of AP-Fcs and AT-Fcs for the enhanced thermal decomposition of AP. Among all the compounds, MAP-Fc showed highest BR catalytic activity for the thermal decomposition of AP. All the above results, concluded that these low-migratory AP-Fcs and AT-Fcs have catalytic effect on thermal decomposition of AP and can be used as BRCs in the AP-based propellant.

Declaration of competing interest

The authors declare that they have no known competing financial interests or personal relationships that could have appeared to influence the work reported in this paper.

Acknowledgment

Financial supports from the National Natural Science Foundation of China (51673170, 5181153009, 21611530689 and 21472168) are gratefully acknowledged.

References

[1] X. Gu, S. Xie, Q. Chen, S. Chen, H. Zhao, Z. Bian, New J. Chem. 42 (2018) 13319–13328.
[2] Z. Deng, H. Yu, L. Wang, X. Zhai, Y. Chen, R. Sun, J. Organomet. Chem. 799 (2015) 273–280.
[3] W. Zhou, L. Wang, H. Yu, X. Xia, Appl. Organomet. Chem. 32 (2018) 1–9.
[4] D. Saravanakumar, N. Sengottuvelan, V. Narayanan, M. Kandaswamy, T.L. Varghese, J. Appl. Polym. Sci. 119 (2011) 2517–2524.
[5] A. Aziz, R. Mamat, W.K.W. Ali, M.R.M. Perang, J. Eng. Appl. Sci. 10 (2015) 6188–6191.
[6] M. Kohga, K. Okamoto, Combust. Flame 158 (2011) 573–582.
[7] J.K. Sharma, P. Srivastava, G. Singh, M.S. Akhtar, S. Ameen, Ceram. Int. 41 (2015) 1573–1578.
[8] X. Fengjuan, S. Minmei, P. Lei, L. Yunjun, Z. Junchai, J. Inorg. Organomet. Polym. 21 (2011) 175–181.
[9] H. Zhao, X. Zhu, Y. Shang, S. Chen, B. Li, Z. Bian, RSC Adv. 6 (2016) 34476–34483.
[10] V.V. Boldyrev, Thermochim. Acta 443 (2006) 1–36.
[11] S.S. Joshi, P.R. Patil, V. Krishnamurthy, Defence Sci. J. 58 (2008) 721–727.
[12] H. Zhao, M. Chen, X. Zhu, S. Chen, Z. Bian, Res. Chem. Intermed. 41 (2015) 3971–3980.
[13] S.M. Shen, S.I. Chen, B.H. Wu, Thermochim. Acta 223 (1993) 135–143.
[14] R. Sun, L. Wang, H. Yu, Z.-u. Abdin, Y. Chen, H. Khalid, N.M. Abbasi, M. Akram, J. Inorg. Organomet. Polym. 24 (2014) 1063–1069.
[15] L. Jiang, M. Liu, L. Xu, T. Dong, J. Li, G. Zhang, Z. Anorg. Allg. Chem. (2018) 1–10.
[16] J. Gao, L. Wang, Y.-l. Tai, J. Wang, J. Huo, A.M. Amin, H. Yu, W. Ding, J. Propul. Power 27 (2011) 1143–1145.
[17] H.-D. Li, Z.-H. Ma, K. Yang, L.-L. Xie, Y.-F. Yuan, J. Mol. Struct. 1024 (2012) 40–46.
[18] B. Wei, Y. Gao, C.X. Lin, H.D. Li, L.L. Xie, Y.F. Yuan, J. Organomet. Chem. 696 (2011) 1574–1578.
[19] M. Saleem, H. Yu, L. Wang, Z.-u. Abdin, H. Khalid, M. Akram, N.M. Abbasi, J. Huang, Anal. Chim. Acta 876 (2015) 9–25.
[20] X. Fan, C. Wang, J. Li, G. Zhang, Z. Anorg. Allg. Chem. 641 (2015) 1169–1175.
[21] E. Shao, D. Li, J. Li, G. Zhang, W. Zhang, Z. Gao, Z. Anorg. Allg. Chem. 642 (2016) 871–881.
[22] Z.-u. Abdin, L. Wang, H. Yu, M. Saleem, M. Akram, N.M. Abbasi, H. Khalid, R. Sun, Y. Chen, New J. Chem. 40 (2016) 3155–3163.
[23] X. Gao, T. An, J. Li, F. Zhao, X. Fan, X. Li, G. Zhang, Z. Gao, Z. Anorg. Allg. Chem. 642 (2016) 155–162.
[24] S.S. Braga, A.M.S. Silva, Organometallics 32 (2013) 5626–5639.
[25] Z.M. Lai, H.M. Ye, Q. Wan, L.L. Xie, S. Bai, Y.F. Yuan, J. Mol. Struct. 1059 (2014) 33–39.
[26] H. Khalid, H. Yu, L. Wang, W.A. Amer, M. Akram, N.M. Abbasi, Z.-u. Abdin, M. Saleem, Polym. Chem. 5 (2014) 6879–6892.
[27] Z. Meng, Z. Wei, K. Fu, L. Lv, Z.-Q. Yu, W.-Y. Wong, J. Organomet. Chem. 892 (2019) 83–88.
[28] Z. Meng, C.-L. Ho, H.-F. Wong, Z.-Q. Yu, N. Zhu, G. Li, C.-W. Leung, W.-Y. Wong, Sci. China Mater. 62 (2019) 566–576.
[29] S.-C. Yiu, A. Nunns, C.-L. Ho, J.H.-L. Ngai, Z. Meng, G. Li, J. Gwyther, G.R. Whittell, I. Manners, W.-Y. Wong, Macromolecules 52 (2019) 3176–3186.
[30] A.W. Orbaek, N. Aggarwal, A.R. Barron, J. Mater. Chem. 1 (2013) 14122–14132.
[31] G. Huang, J. Weng, Curr. Org. Chem. 15 (2011) 3653–3666.
[32] P. Molina, A. Tarraga, M. Alfonso, Dalton Trans. 43 (2014) 18–29.
[33] M. Alfonso, A. Espinosa, A. Tarraga, P. Molina, Chem. Commun. 48 (2012) 6848–6850.
[34] S.R. Beeren, J.K.M. Sanders, J. Am. Chem. Soc. 133 (2011) 3804–3807.
[35] Z. Meng, F. Xiao, Z. Wei, X. Guo, Y. Zhu, Y. Liu, G. Li, Z.-Q. Yu, M. Shao, W.-Y. Wong, Nano Res. 12 (2019) 2954–2959.
[36] Q. Dong, Z. Meng, C.-L. Ho, H. Guo, W. Yang, I. Manners, L. Xu, W.-Y. Wong, Chem. Soc. Rev. 47 (2018) 4934–4953.
[37] M. Drusan, R. Sebesta, Tetrahedron 70 (2014) 759–786.
[38] D.J. Young, S.W. Chien, T.S.A. Hor, Dalton Trans. 41 (2012) 12655–12665.
[39] D. Schaarschmidt, H. Lang, Organometallics 32 (2013) 5668–5704.
[40] V.H. Purecha, N.S. Nandurkar, B.M. Bhanage, J.M. Nagarkar, Tetrahedron Lett. 49 (2008) 5252–5254.

[41] Z. Cheng, G. Zhang, X. Fan, F. Bi, F. Zhao, W. Zhang, Z. Gao, Inorg. Chim. Acta. 421 (2014) 191–199.
[42] R. Kurane, V. Gaikwad, J. Jadhav, R. Salunkhe, G. Rashinkar, Tetrahedron Lett. 53 (2012) 6361–6366.
[43] M. Liu, E. Shao, K. Zhao, J. Li, Z. Gao, G. Zhang, Z. Anorg. Allg. Chem. 643 (2017) 802–810.
[44] K. Subramanian, J. Polym. Sci., Polym. Chem. Ed. 37 (1999) 4090–4099.
[45] J. Li, X. Gao, E. Shao, G. Zhang, Z. Anorg. Allg. Chem. 643 (2017) 455–463.
[46] X. Liu, D. Zhao, F. Bi, X. Fan, F. Zhao, G. Zhang, W. Zhang, Z. Gao, J. Organomet. Chem. 762 (2014) 1–8.
[47] T. Li, D. Li, J. Li, G. Zhang, W. Zhang, Z. Gao, Z. Anorg. Allg. Chem. 642 (2016) 1095–1103.
[48] P. Povea, J.L. Arroyo, G. Carreño, Á. Norambuena, P.L. Rios, M.B. Camarada, I. Chavez, J.M. Manriquez, C. Morales-Verdejo, Thermochim. Acta 666 (2018) 181–189.
[49] C. Morales-Verdejo, M.B. Camarada, J.L. Arroyo, P. Povea, G. Carreño, J.M. Manriquez, J. Therm. Anal. Calorim. 131 (2018) 353–361.
[50] C. Wang, J. Li, X. Fan, F. Zhao, W. Zhang, G. Zhang, Z. Gao, Eur. J. Inorg. Chem. 2015 (2015) 1012–1021.
[51] Z. Cheng, G. Zhang, X. Fan, F. Bi, F. Zhao, W. Zhang, Z. Gao, Inorg. Chim. Acta. 421 (2014) 191–199.
[52] X. Liu, W. Zhang, G. Zhang, Z. Gao, New J. Chem. 39 (2015) 155–162.
[53] Z.-u. Abdin, H. Yu, L. Wang, M. Saleem, H. Khalid, N.M. Abbasi, M. Akram, Appl. Organomet. Chem. 28 (2014) 567–575.
[54] P.J. Swarts, M. Immelman, G.J. Lamprecht, S.E. Greyling, J.C. Swarts, S. Afr. J. Chem. 50 (1997) 208–216.
[55] Z.-u. Abdin, L. Wang, H. Yu, R.U. Khan, R.S. Ullah, M. Haroon, Appl. Organomet. Chem. 32 (2018) 1–11.
[56] Y. Gao, H.D. Li, C.F. Ke, L.L. Xie, B. Wei, Y.F. Yuan, Appl. Organomet. Chem. 25 (2011) 407–411.
[57] Z.M. Lai, H.M. Ye, Q. Wan, L.L. Xie, S. Bai, Y.F. Yuan, J. Mol. Struct. 1059 (2014) 33–39.
[58] J. Li, C. Wang, X. Gao, F. Zhao, K. Zhao, X. Fan, G. Zhang, W. Zhang, Z. Gao, Polyhedron 106 (2016) 58–64.
[59] M. Saleem, L. Wang, H. Yu, M. Akram, R.S. Ullah, Colloid Polym. Sci. 295 (2017) 995–1006.
[60] M. Saleem, H. Yu, L. Wang, Z.-u. Abdin, H. Khalid, M. Akram, N.M. Abbasi, Y. Chen, J. Electroanal. Chem. 763 (2016) 71–78.
[61] Z.-u. Abdin, L. Wang, H. Yu, M. Saleem, M. Akram, H. Khalid, N.M. Abbasi, R.U. Khan, Appl. Organomet. Chem. 31 (2017) 1–10.
[62] Z.-u. Abdin, L. Wang, H. Yu, M. Saleem, M. Akram, H. Khalid, N.M. Abbasi, X. Yang, J. Colloid Interface Sci. 487 (2017) 38–51.
[63] W. Zhou, L. Wang, H. Yu, A. Zain ul, X. Yang, Q. Chen, J. Wang, RSC Adv. 6 (2016) 53679–53687.
[64] X. Wang, L. Wang, H. Zou, W. Qian, Y. Liao, Colloid Polym. Sci. 293 (2015) 2027–2034.
[65] R. Solmaz, G. Kardaş, Prog. Org. Coating 64 (2009) 81–88.
[66] H. Çiftçi, H.N. Testereci, Z. Öktem, Polym. Bull. 66 (2011) 747–760.
[67] D. Mohanty, Synthesis and Characterization of the Polymeric Phenolic Schiff Bases Containing Aminothiazole Moiety, 2014.
[68] M. Bıyıkoğlu, H. Çiftçi, Polym. Bull. 70 (2013) 2843–2856.
[69] P. Samadhiya, R. Sharma, S.K. Srivastava, S.D. Srivastava, J. Serb. Chem. Soc. 77 (2012) 599–605.
[70] Y. Bide, M.R. Nabid, F. Dastar, RSC Adv. 5 (2015) 63421–63428.
[71] S. Ramalingam, S. Periandy, S. Mohan, Spectrochim. Acta 77 (2010) 73–81.
[72] S. Akyüz, J. Mol. Struct. 449 (1998) 23–27.
[73] M. Yıldırım, İ. Kaya, Synth. Met. 162 (2012) 436–443.
[74] L. Jiang, M. Liu, L. Xu, T. Dong, J. Li, G. Zhang, Z. Anorg. Allg. Chem. 645 (2019) 92–100.
[75] X. Liu, J. Li, F. Bi, W. Zhang, G. Zhang, Z. Gao, Eur. J. Inorg. Chem. 2015 (2015) 1496–1504.
[76] J. Li, L. Jiang, D. Jia, L. Xu, G. Zhang, Z. Anorg. Allg. Chem. 645 (2019) 14–21.
[77] A. Khan, H. Yu, Y. Wang, L. Wang, R.S. Ullah, F. Haq, T. Elshaarani, M. Usman, A. Nazir, K.-u.-R. Naveed, J. Organomet. Chem. 902 (2019) 120955.
[78] L. Ma, L. Wang, Q. Tan, H. Yu, J. Huo, Z. Ma, H. Hu, Z. Chen, Electrochim. Acta 54 (2009) 5413–5420.
[79] Q. Tan, L. Wang, L. Ma, H. Yu, Q. Liu, A. Xiao, Macromolecules 42 (2009) 4500–4510.
[80] C. Li, L. Wang, L. Deng, H. Yu, J. Huo, L. Ma, J. Wang, J. Phys. Chem. B 113 (2009) 15141–15144.
[81] Q. Tan, L. Wang, L. Ma, H. Yu, J. Ding, Q. Liu, A. Xiao, G. Ren, J. Phys. Chem. B 112 (2008) 11171–11176.
[82] H. Yu, L. Wang, J. Huo, C. Li, Q. Tan, Des. Monomers Polym. 12 (2009) 305–313.
[83] T. Chen, L. Wang, G. Jiang, J. Wang, X.j. Wang, J. Zhou, J. Wang, C. Chen, W. Wang, H. Gao, J. Electroanal. Chem. 586 (2006) 122–127.
[84] A. Bard, L. Faulkner, Electrochemical Methods Fundamentals and Applications, John Wiley & Sons, New York, 2001.
[85] Q. Yang, S. Chen, G. Xie, S. Gao, J. Hazard Mater. 197 (2011) 199–203.
[86] W. Zhou, L. Wang, H. Yu, R. Tong, Q. Chen, J. Wang, X. Yang, Z.-u. Abdin, M. Saleem, Appl. Organomet. Chem. 30 (2016) 796–805.
[87] R. Tong, Y. Zhao, L. Wang, H. Yu, F. Ren, M. Saleem, W.A. Amer, J. Organomet. Chem. 755 (2014) 16–32.
[88] Y. Yuan, W. Jiang, Y. Wang, P. Shen, F. Li, P. Li, F. Zhao, H. Gao, Appl. Surf. Sci. 303 (2014) 354–359.